Open access • Proceedings Article • DOI:10.1109/MED.2017.7984315

Novel considerations on the negative pressure adhesion of electric ducted fans: An experimental study — Source link

Angelica Brusell, George Andrikopoulos, George Nikolakopoulos

Institutions: Luleå University of Technology

Published on: 01 Jul 2017 - Mediterranean Conference on Control and Automation

Novel Considerations on the Negative Pressure Adhesion of Electric Ducted Fans: An Experimental Study

Angelica Brusell, George Andrikopoulos, and George Nikolakopoulos

***Abstract*— In this article, the potential of utilizing an Electric Ducted Fan (EDF) as an adhesion actuator is investigated in detail, where an experimental setup is implemented for evaluating the EDF's ability to adhere to a test surface through negative pressure generation. Different design variables and modifications to the original EDF structure are tested, while their impact on the adhesion efficiency is experimentally evaluated. The presented investigation acts as a preliminary study to the goal of incorporating the resulting optimized negative pressure-based actuation method in a wall-climbing robot for inspection of aircraft fuselages.**

I. INTRODUCTION

Electric Ducted Fans (EDFs) have been traditionally popular for their utilization as a propulsion method for both big and small-scale aircrafts, mainly due to an increased thrust efficiency by the ducts reduction of tip vortices and the pressure drops at the blade tips, when compared to their open air equivalents [1]. A typical EDF design, as graphically displayed in Fig. 1, consists of a motor and an impeller, encased by a cylindrical duct and shroud. A rotor and aft cone are usually incorporated to reduce the turbulence of the air flow through the duct around the motor.

However, the utilization of EDFs has not been limited to propelling a craft through air, as their ability to generate a negative pressure and actively adhere to a surface, when their ducted structure is placed at a close proximity[2] [3], has led to different application areas, with the most recent being the Wall-Climbing Robots (WCRs) [4].

Although the WCRs presented in the related literature have been utilizing a number of different methods for adhesion, from passive [5] [6] and active suction cups [7] [8] to vortex chambers [2] [9] and magnetic attraction [10] [11], the use of an EDF-based design, as an adhesion method, provides important advantages that could increase the potential usability of WCRs, has not been addressed yet at full extent.

Specifically, EDFs do not require the adhesion mechanism to be in contact with the target surface, which alleviates the design challenges of adhesion in cases of curved, rough or non-magnetic target surfaces [2]. In addition, such a design technique has an impact on the overall cost, since no external equipment (e.g. compressor, filters, tubes etc.) have to be used, which produces a untethered-friendly solution.

This work has received funding from the European Unions H2020 Framework Programme under the call FET-OPEN, grant agreement No. 665238.

A. Brusell, G. Andrikopoulos and G. Nikolakopoulos are with the Robotics Team at Control Engineering Group, LuleåUniversity of Technology, SE-97189 Luleå, Sweden.

Corresponding Author's Email:angbru@ltu.se

Fig. 1. Typical EDF design in assembled and exploded view

In the small number of applications found in related literature that utilize an EDF-based design, the main research aspect has been either the negative pressure generation [2], or thrust [12] [3] generated by the EDF. From this related work it becomes apparent that the experimental evaluation has been constrained on investigating the effect of the distance of the EDF shroud to the target surface, on the adhesion efficiency. Thus, there is an identified gap on the investigation of important design parameters, such as the EDF's placement, the length and dimensions of the duct, the dimensions of the shroud and its distance from the surface, which complicates the modeling and control of such a system.

The main contribution of this article stems from the experimental evaluation of the potential of utilizing a commercially available EDF as an adhesion mechanism, while providing a novel insight on the analysis of the adhesion nature related to negative pressure and thrust force generation against a target surface. To this goal, a novel experimental setup for the EDF testing is proposed for acquiring important properties such as adhesion force and generated pressure during the EDF's operation when placed against a test surface. In addition, this article will also contribute towards the novel evaluation of different design variables and modifications to the original EDF structure for their effect on the adhesion efficiency and the dependence of the adhesion nature to the EDF's distance from the test surface.

The rest of this article is structured as follows. II covers the fundamental negative pressure adhesion principles, while

Section III presents the experimental setup's design specifics and utilized components. In Section IV the experimental results are presented in detail and finally, the concluding remarks are provided in Section V.

II. NEGATIVE PRESSURE ADHESION PRINCIPLE

Negative pressure adhesion works on the principle of generating and maintaining a low pressure zone P_a inside a cavity compared to the surrounding outside pressure P_b. As depicted in Fig. 2, the difference in pressure will induce a force F_s across the projected cavity area onto the target surface, A, by the high pressure region [13] as:

$$F_s = A(P_b - P_a). \tag{1}$$

Considering an EDF-based adhesion mechanism, the low pressure zone lies within its shroud, hence the active pressure area is $A = \pi(r_s^2 - r_d^2)$ mm^2 with r_s and r_d denoting the outer shroud radius and the duct's internal radius, respectively. In this definition, the effect of the shroud's curvature is neglected for simplification purposes. Area A will from now on be referred to as the active area. In this configuration, an increase in applied force can occur via a decrease in the shroud's pressure, or an increase in the active area.

Furthermore, air flow through the low pressure zone P_a is introduced by the distance between the shroud's end and the test surface, h, as displayed in Fig. 2. The flows Q_{in} and Q_{out} entering and exiting the chamber are defined by,

$$\begin{aligned} Q_{in} &= A_{in} v_{in}, \\ Q_{out} &= A_{out} v_{out}, \end{aligned} \tag{2}$$

where A_{in} and A_{out} denote the in- and outlet areas, while v_{in} and v_{out} denote the air velocity into and out of these areas. The outlet area is $A_{out} = \pi(r_d^2 - r_m^2)$ mm^2, with r_m denoting the radius of the motor's cylindrical case, while the inlet area $A_{in} = 2\pi h r_s$ mm^2 depends on the gap height h.

In order for a negative pressure zone to be generated, the flow out of the chamber has to be higher than the flow in, for a specific period of time. As P_a lowers, air is pulled in through the gap and after a time t the flow reaches an equilibrium, with the lower pressure zone being maintained. The steady state operational point is defined as:

$$A_{in} v_{in} = A_{out} v_{out}, \tag{3}$$

In other words, a mass flow imbalance occurs for an increase in the EDF's rotational speed. As air is drawn out from A_{out} at a faster rate than in through A_{in}, this results in an additional pressure decrease in the inlet area, which is defined as the air volume constrained by the shroud and its projection to the target surface. This decrease in pressure will speed up the air flowing in through the gap until a steady-state is reached, while as the rotational speed is kept constant the negative pressure and flow rates remain constant as well.

In addition to the adhesion force produced through the negative pressure, the EDF will generate a thrust as it pulls air through the duct. At small h, the air density will not be enough to create a big thrust force, but as the gap increases and airflow is less restricted, the generated thrust will increase. Ultimately the thrust generated will converge to its free flight equivalent [14].

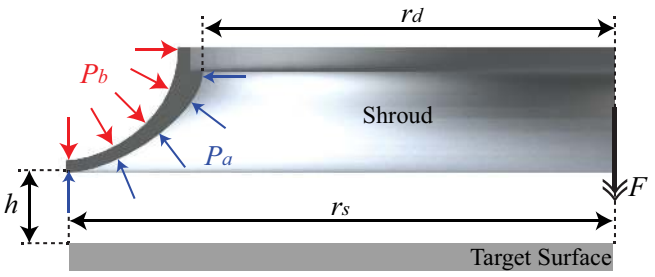

Fig. 2. Shroud detail in half-section view with highlighted shroud pressure zones and geometrical properties.

III. EXPERIMENTAL SETUP

A. Conceptual Design Properties

The experimental setup was designed with the main goal of measuring the adhesion force F exerted from the EDF to the test surface. To achieve this, as represented in Fig. 3, the EDF was mounted to a legged support structure where each of the four legs was connected to the baseplate via a load cell, resembling the rectangular formation of commercial weight scales. In this configuration, the total measured force F will be derived by the summation of the force measured by the four load cells, displayed in Fig. 3 as $F_{1,\dots,4}$.

In the setup's conceptual design presented in Fig. 3, a vacuum sensor array was placed underneath the test surface with the sensing tips placed coincidently through inlet holes of the surface. Provided the general symmetry of the EDF structure, the flow distribution along circular sections around the EDFs longitudinal axis in its interior and exterior space was assumed to be symmetrical, while the aerodynamic effect of the legged structure was assumed negligible. For these reasons, the sensor array was placed radially from the surface center, which is defined as the intersection of the EDF's longitudinal axis and the target surface. In this way, the setup provides with a series of pressure sensor points, denoted in Fig. 3 as $P_{1,\dots,8}$. A ninth sensor P_9 was placed at the top of the EDF duct for reference purposes and to provide an insight on the generated thrust.

In order to expand the evaluation span of the EDF's adhesion properties, different design variables in the setup were incorporated. Specifically, the distance of the EDF from the test surface h_j was conceptualized as variable and to this purpose the legged structure was equipped with multiple inlets placed at predetermined intervals denoted by the subscript j. In addition, EDF shrouds of different outer diameter r_s were designed to be interchangeable via mounting brackets for evaluating the effect of the active surface and volume change on the attraction between the EDF and the test surface for a given distance. For the needs of this study, the design of the shrouds followed the outward curvature profile utilized in commercially available EDFs, while their height l was selected as constant and predefined.

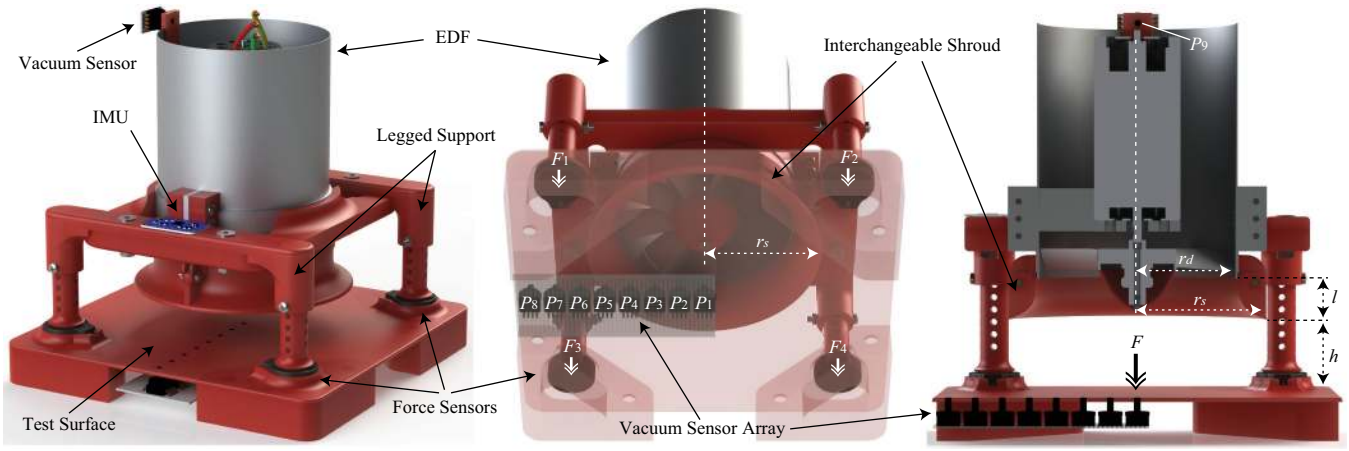

Fig. 3. Graphical representation of the Experimental setup: side (left) and bottom semi-transparent (middle) view with highlighted sensor components, (right) half-section view with highlighted design variables.

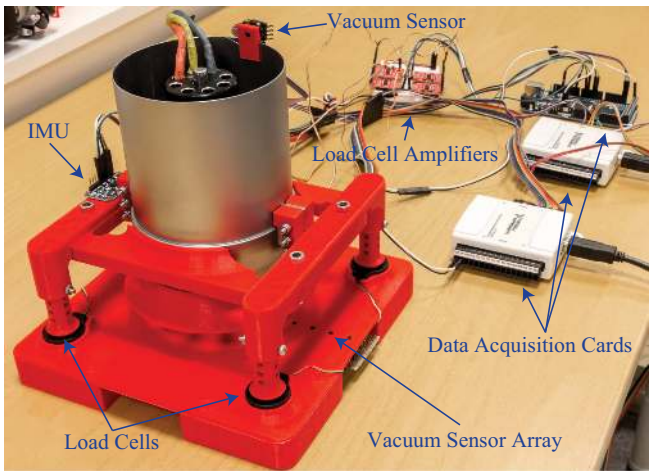

Fig. 4. Experimental setup prototype with highlighted sensor and data acquisition components.

B. Setup Prototype and Utilized components

The setup prototype, which is displayed in Fig. 4, was 3D printed from polylactide (PLA) following the required design properties for the execution of this study. The dimensions were adjusted to the needs of the selected test-EDF and sensors. Specifically, the test surface was printed as a 190×190×2 mm (Length×Width×Height) plate, with incorporated inlet holes for the pressure sensors and mount extrusions for the load cells. The gap height h can be set between 3 and 21 mm in 3 mm increments. This is achieved via the inlet holes of the structure's four legs, placed in a 140×140 mm formation for uniform force distribution.

The test-EDF selected for the needs of the presented study is a commercially available model developed by Dr. MadThrust Co. with inner duct diameter at 92 mm, overall weight 0.67 kg and 12-blade fan actuated via a brushless DC motor of 2350 W maximum power at 41000 maximum rpm, which provides a maximum thrust of 3.8 kg. The Electronic Speed Controller (ESC) selected for this EDF unit was the Turnigy AE-100A with continuous current capability of 100 A and is characterized by a fast and precise throttle response.

The EDF's aluminum shroud was replaced by three different EDF shrouds, which were 3D printed via polylactide (PLA) with r_s = 60, 70 and 80 mm, following an outward curvature profile and constant shroud thickness 2 mm, while all the shroud heights were predefined at l = 22 mm. For measuring the force F generated from the EDF and acted on the test surface via the legged structure, four TE Connectivity button-type load cells, with 11.34 kg maximum range, were utilized and properly incorporated in both the test-surface and respective leg tips in order to ensure proper uniformal tension on the active button element of each force sensor and thus more reliable measurements.

The acquisition of the negative pressure measurements was achieved via multiple NXP USA Inc. MPXV5050V differential pressure sensors with a sensing range of up to -50 kPa. Due to the differential principle of their operation, the tip sensing point targets the test surface while their capsule reference point remains in a part of the setup unaffected by the flow. Specifically, a sensor array of eight sensors was placed in a single radial formation along the test surface; starting from the surface center, i.e. the intersection of the test surface with the EDF's longitudinal axis, the sensors we placed radially at a 12.5 mm interval that was dictated by the sensor dimensions. A ninth sensor of the same type was also placed at the top of the EDF duct.

A LSM9DS0 Inertial Measurement Unit (IMU) was utilized for the measurement of the vibrations on the legged setup via its integrated accelerometer, while its temperature sensor was used to monitor the thermal levels of the setup and ensure the EDF's safe operation during the experimental sequences. Finally, the EDF's operation and the acquisition of the setup's sensorial data were achieved via two National Instruments USB-6008 cards and one Arduino Mega, while the setup's programming was carried out in MATLAB.

IV. EVALUATION OF VORTEX ADHESION PROPERTIES

In this section, experimental sequences were performed for different combinations of r_s and h values, with the throttle T input signal being a stepping function of 5 % increments

every 5 seconds, until a peak throttle T_{max} = 80 % was reached and the procedure then reversed down and reaching T = 0 %. Ten seconds of data was collected before and after the throttle step signal to ensure the calibration integrity of the sensors during every experiment. The upper limit of 80 % was set via the ESC for safety against overheating. Force measurements are acquired as the summation of the four load cells, while subtracting the weight of the EDF equipment acting on the force measurements points in order to properly extract the adhesion force measurement.

The points $P_i, i = 1, \ldots, 8$, denote the vacuum sensors radially and outwards from the surface center, starting with P_1 as the center sensing point. It is important to note that for the variable shroud radii r_s, the sensors lying under the EDF and shroud differ. Specifically, for r_s = 60, 70 and 80 mm the sensors $P_{1,\ldots,5}$, $P_{1,\ldots,6}$ and $P_{1,\ldots,7}$ lie within the outer radius, respectively. In all aforementioned cases, $P_{1,\ldots,3}$ are positioned under the EDF duct, while the respective remaining sensing points are positioned under the shroud. The test setup was properly designed so that there are always sensors outside the affected surface area, in order to provide an insight on how the pressure is affected in these cases.

An indicative experimental test was executed using the r_s = 70 mm and h = 6 mm, while the acquired throttle input T, negative pressure P_i, force F and supplied current I are presented in Fig. 5. A clear increase in negative pressure is observed with the increase in throttle, which becomes progressively greater for the pressure sensors closer to the surface center, thus reflecting the generation of a vortex.

The maximum negative pressures were recorded for the center point P_1, reaching a maximal value of approximately 6.5 kPa for T = 80 %. The neighboring sensor P_2 is providing similar measurements but its larger range profile appearing as noise, reveals the different effect from the vortex generation. On the opposite side, the sensors P_7 and P_8, which are positioned outside of the affected area of the chosen shroud, measure a smaller pressure change as the air volume is bigger and the inlet area restricted, but the entirety of the low pressure zone is thus not confined to just the volume between the shroud and the surface, but extends further and outside the enclosed volume. The measured force F shows a behavior proportional to the throttle, following the quick response characteristics of the negative pressure signals with absence of transient phenomena. As expected, the maximum force was acquired for maximum throttle and was measured at around 21 N.

The aforementioned experimental trial provided a clear indication of the generated vortex and the resulting adhesion, as already recorded in related literature [2]. The experimental cases presented in the sequel were performed in order to a) find the design variables that provide this EDF setup's optimal performance, and b) investigate whether the vortex is the evident and sole factor for generating adhesion in all shroud and gap height cases.

Specifically, the aggregated P_n and F results for h = 3, ..., 12 mm and r_s = 60, 70, 80 mm were acquired and are displayed in Fig. 5 for the same maximum throttle input

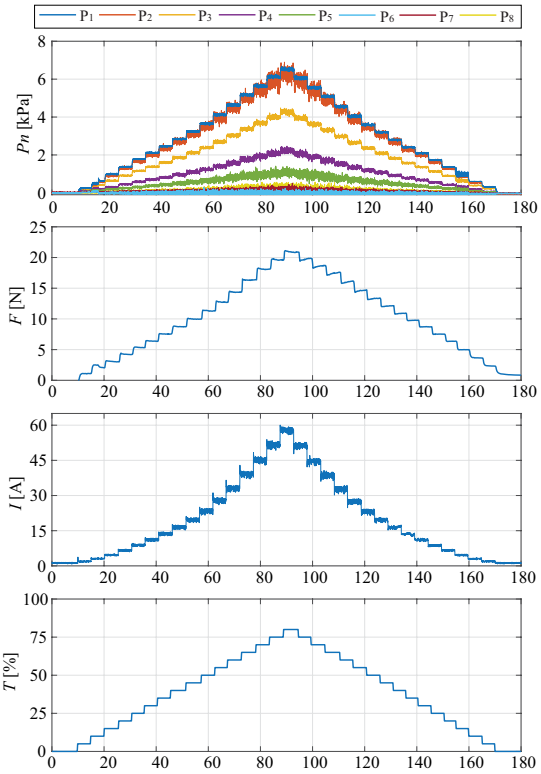

Fig. 5. Experimentally acquired negative pressure, force and current responses along with the input throttle signal T for the case of r_s = 70 mm and h = 6 mm.

signal. For all presented cases of different gap heights and shrouds the negative pressure and measured force follow a proportional nature to the increase and decrease in throttle, with the maximum measurements acquired at maximum throttle (80%). An important observation is that the increase in the gap height leads to a clear decrease in the P_n measurements, but the force does not follow the same decreasing behavior. On the contrary, the force increases to a maximum of approximately 55 N in the case of h = 15 mm and r_s = 80 mm. This reveals a change in adhesion nature that reflects a pressure distribution change in need of further analysis.

To investigate this phenomenon, the experiments were repeated for all combinations of r_s = 60, 70 and 80 mm and h = 3 to 21 mm with 3 mm increments with the same throttle input signal. The surface pressure distribution P_n with respect to the radial distance from the surface center (in mm), which concede with the pressure sensor points, for all gap heights h and shroud radii r_s are presented in Fig. 6. These results show an increasing behavior as the shroud radius increases and indicate a clear change in pressure distribution as the gap alters, with an evident dissipation of the vortex phenomenon and a general decrease in P_n for increasing h values. This change in distribution emphasized by the maximum pressures is rapidly progressing for all shrouds in gaps between 6 and 12 mm, where the increase in h shifts the dominant pressure points from the near-center ones $P_{1,2,3}$ to the middle $P_{4,5,6}$.

To visualize this complex phenomenon and its rapid progression, the experimentally acquired pressure distribution is

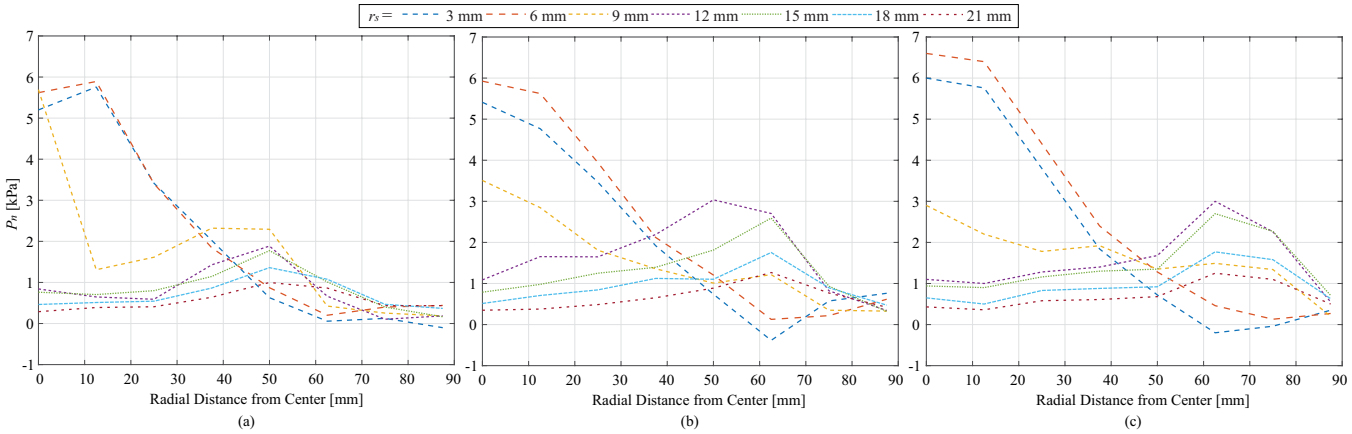

Fig. 6. Measured pressure distributions at maximum T = 80 % for h = 3 to 21 mm with 3 mm increments and for r_s = (a) 60, (b) 70 and (c) 80 mm.

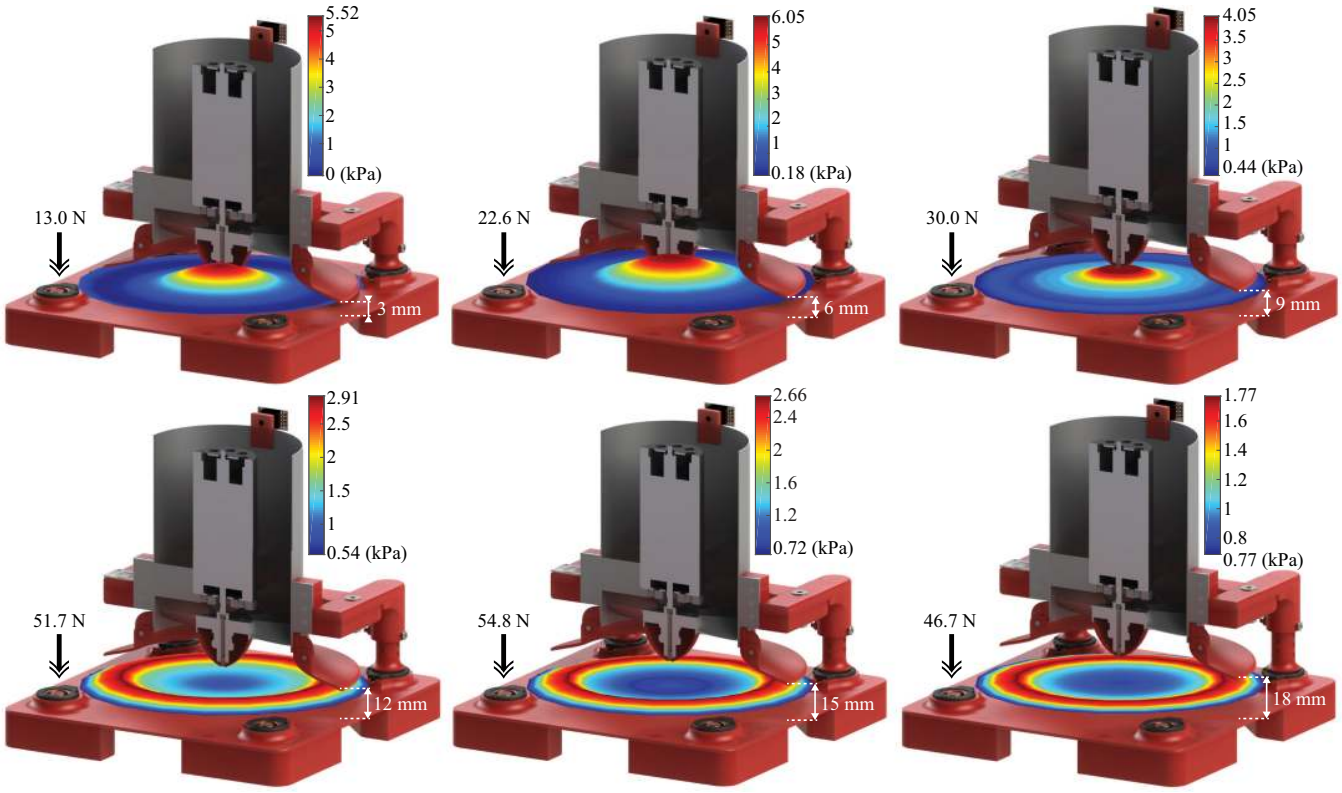

Fig. 7. Graphical representation of the experimentally acquired pressure distribution on the test surface for constant T = 80 %, r_s = 80 mm and gaps h = 3 to 18 mm with 3 mm increments).

radially expanded to the affected test surface for the shroud case of r_s = 80 mm, for T = 80 % and gap heights of h = 3, ..., 18 mm with 3 mm increments. As displayed in Fig. 7, the pressure values are visualized via different coloring, the values of which are presented in color bars for all respective cases, while the maximum mean force is also indicated. As mentioned, there is a fast progression when the gap reaches 9 mm, where the centralized vortex pressure profile dissipates and gets shifted from the area underneath the duct towards the outer surface area beneath the shroud.

As the gap increases, the negative pressure distribution gets minimized from a range of 0 - 5.32 kPa at h = 3 mm to 0.77 - 1.77 kPa at h = 18 mm, but the force undergoes a big increase from 13 to 46.7 N. This observation leads to the conclusion that the occurring vortex is not the sole factor for adhesion to the test surface. Specifically, as h increases above a specific threshold, the inflow of air increases suddenly and starts to get propelled through the duct, thus producing thrust. This abrupt change was experimentally observed by a sudden and large increase in sensed flow, which was accompanied by increased noise and vibrations.

Thus, the produced thrust results in an additive force component that leads to the observed increase in the measured force summation. Further increase of the gap height would lead to the EDF reaching a adhesion force plateau and generating thrust converging to its free flight equivalent,

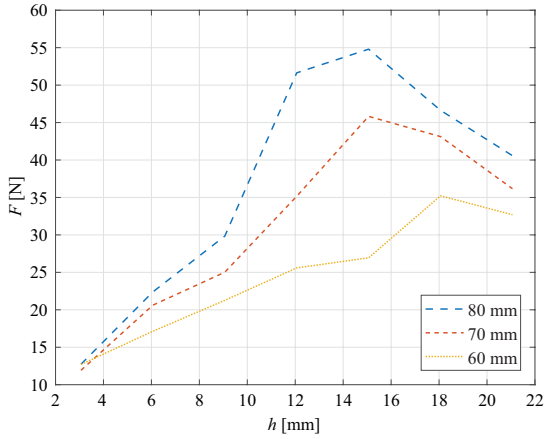

Fig. 8. Maximum measured force in relation to the gap height for the three different shrouds.

while the vortex phenomenon is no longer observed. This observation provides an important insight to future modeling of these two additive phenomena and presents a novel design strategy for achieving optimal adhesion performance.

The above observation is also visible in Fig. 8, which displays the maximum mean force measurements extracted for all three shrouds and for all available gaps. As expected, an increase in r_s leads to an increase in maximum mean force measured for all h values, which agrees with 1, given the increase in the active area A. For each r_s = 60, 70 and 80 mm case, F reaches its maximal state of 35.4, 45.9 and 54.8 N at h = 18, 12 and 15 mm, respectively. This increase is translated as approximately 272, 353 and 421 % compared to the initial adhesion force generated at h = 3 mm. At this initial gap of 3 mm, the force measurement is observed to be the numerically identical for all three shrouds, leading to the conclusion that in cases of very small gaps the shroud size does not have any effect on the adhesion efficiency, as the negative pressure is concentrated in the center of the surface, rather than under the active area defined in Fig. 2. Finally, h values higher than 15 mm lead to a decrease in force, thus highlighting the vortex dissipation.

V. CONCLUSIONS

In this article, the negative pressure adhesion properties of an Electric Ducted Fan (EDF) was experimentally evaluated. The goal of this study was the structural optimization of the EDF's adhesion efficiency for its future incorporation in a wall-climbing robot for inspection purposes. To this goal, an experimental setup was designed and developed for measuring the pressure distribution and adhesion force generated when an EDF is placed at close proximity to a test surface. Variable design characteristics regarding shroud radii and distances from the target surface were investigated in order to determine their structural impact on the generated adhesion force responses.

A series of experimental sequences was performed, which showed that an increase in shroud outer radii results to an increase in pressure and force for a given gap height. An important observation was made when the gap heights were increased, as the pressure distribution along the test surface changed in form and decreased in intensity, whereas the adhesion force was greatly increased.

The proposed methodology revealed the additive nature of a thrust force component, which was occurring abruptly after exceeding a specific gap threshold and was leading to large increase in adhesion efficiency ranging between 272 - 421 % compared to the initial adhesion force generated at small gap heights. At these small gaps, it was observed that the shroud size does not have any effect on the adhesion efficiency, as the negative pressure is concentrated in the center of the surface, rather than the area under the shroud.

The presented study and produced results will act as a new knowledge basis on EDF-based designs and the cornerstone for future modeling, identification and control approaches, with the goal of incorporating the resulting optimized negative pressure-based actuator in a WCR design for inspection.

REFERENCES

[1] B. R. W. Abrego, Anita I., "Performance Study of a Ducted Fan System," *American Helicopter Society Aerodynamics, Acoustics, and Test and Evaluation Technical Specialists Meeting, San Francisco, CA.*, 2002.

[2] J. X. J. Xiao, A. Sadegh, M. Elliott, A. Calle, A. Persad, and H. M. C. H. M. Chiu, "Design of Mobile Robots with Wall Climbing Capability," *Proceedings, 2005 IEEE/ASME International Conference on Advanced Intelligent Mechatronics.*, pp. 24–28, 2005.

[3] J. Xiao, B. Li, K. Ushiroda, and Q. Song, "Rise-Rover : A Wall-Climbing Robot with High Reliability and Load-Carrying Capacity," *Proceedings of the 2015 IEEE Conference on Robotics and Biomimetics*, pp. 2072–2077, 2015.

[4] A. Brusell, G. Andrikopoulos, and G. Nikolakopoulos, "A Survey on Pneumatic Wall-Climbing Robots for Inspection," in *24th Mediterranean Conference on Control and Automation (MED)*, 2016.

[5] S. Kawasaki and K. Kikuchi, "Development of a Small Legged Wall Climbing Robot with Passive Suction Cups," in *The 3rd International Conference on Design Engineering and Science, ICDES 2014*, 2014, pp. 112–116.

[6] Y. Yoshida and S. Ma, "Design of a Wall-Climbing Robot with Passive Suction Cups," *2010 IEEE International Conference on Robotics and Biomimetics*, pp. 1513–1518, 2010.

[7] J. Shang, T. Sattar, S. Chen, and B. Bridge, "Design of a climbing robot for inspecting aircraft wings and fuselage," *Industrial Robot: An International Journal*, vol. 34, no. 6, pp. 495–502, 2007.

[8] R. Pack, "A rubbertuator-based structure-climbing inspection robot," *IEEE Intemational Conference on Robotics and Automation*, no. April, pp. 1869–1874, 1997.

[9] Q. Zhou and X. Li, "Design of Wall-climbing Robot Using Electrically Activated Rotational-flow Adsorption Unit," *2016 IEEE/RSJ International Conference on Intelligent Robots and Systems (IROS)*, pp. 5758–5763, 2016.

[10] Y. Zhang, T. Dodd, K. Atallah, and I. Lyne, "Design and Optimization of Magnetic Wheel for Wall and Ceiling Climbing Robot," *2010 IEEE International Conference on Mechatronics and Automation*, pp. 1393–1398, 2010.

[11] Z. Bi, Y. Guan, S. Chen, H. Zhu, and H. Zhang, "A miniature biped wall-climbing robot for inspection of magnetic metal surfaces," *2012 IEEE International Conference on Robotics and Biomimetics (ROBIO)*, pp. 324–329, 2012.

[12] P. Sekhar and R. Bhooshan, "Duct Fan Based Wall Climbing Robot for Concrete Surface Crack Inspection," *IEEE India Conference (INDICON)*, 2014.

[13] Y. Guan, H. Zhu, W. Wu, X. Zhou, L. Jiang, C. Cai, L. Zhang, and H. Zhang, "A Modular Biped Wall-Climbing Robot With High Mobility and Manipulating Function," *IEEE/ASME Trans. Mechatronics*, vol. 18, no. 6, pp. 1787–1798, 2013.

[14] R.A.Sharman, "Electric Ducted Fan theory and practice," 2013. [Online]. Available: http://www.rcgroups.com/forums/showatt.php?attachmentid=6384145